**Proceedings of the ASME 2011 International Design Engineering Technical Conferences &
Computers and Information in Engineering Conference
IDETC/CIE 2011
August 28-31, 2011, Washington, DC, USA**

DETC2011-47968

ON THE DYNAMICS OF TWO MUTUALLY-COUPLED, ELECTROMAGNETICALLY-ACTUATED MICROBEAM OSCILLATORS

Andrew B. Sabater, Jeffrey F. Rhoads*
School of Mechanical Engineering,
Birck Nanotechnology Center,
and Ray W. Herrick Laboratories
Purdue University
West Lafayette, Indiana 47907
Email: jfrhoads@purdue.edu

ABSTRACT

This work describes the modeling, analysis, predictive design, and control of self-excited oscillators, and associated arrays, founded upon electromagnetically-actuated microbeams. The study specifically focuses on the characterization of nonlinear behaviors arising in isolated oscillators and small arrays of nearly-identical, mutually-coupled oscillators. The work provides a framework for the exploration of larger oscillator arrays with different forms of coupling and feedback, which can be exploited in practical applications ranging from signal processing to micromechanical neurocomputing.

1 INTRODUCTION

Though studies of simple oscillators, self-excited systems with a stable amplitude and neutrally stable phase, date back centuries, these systems remain a topic of great interest, due in part to their utility in micro- and nanoscale timing applications [1–5]. While engineering research interest has largely focused on isolated oscillator systems, coupled arrays of oscillators can have vastly different (and typically more complex) dynamics, as demonstrated in a number of interesting studies produced by the applied mathematics, physics, and biology communities [5–16]. While efforts in these fields have addressed a wide variety of research questions, there remains a number of open questions related to the existence and stability of emergent behaviors, such as synchronization, as well as the active exploitation of these dynamic behaviors in practical application. At the microscale, Hoppensteadt and Izhikevich have proposed the use of coupled oscillators in neurocomputing [17]. Likewise, Chang et al. have demonstrated that certain coupled oscillator topologies can be used in development of reduced phase noise electronics [18]. The goal of the current study is to build upon these efforts through the modeling, analysis, predictive design, and control of self-excited oscillators, and associated arrays, founded upon electromagnetically-actuated microbeams. With proper development, the authors believe these systems have distinct potential in mass sensing, signal processing, and computing applications.

This work begins in Section 2 with the development of a distributed-parameter model for a representative electromagnetically-actuated microbeam resonator, and the subsequent reduction of this model to a lumped-parameter analog. Section 3 presents a nonlinear control law for self-excitation, and the analysis of related nonlinear behaviors. Section 4 considers the dynamics of two mutually-coupled nearly-identical oscillators, and the work concludes with a brief discussion of potential applications and future work.

*Address all correspondence to this author.

2 ISOLATED ELECTROMAGNETICALLY-ACTUATED MICROBEAM MODEL

The device under consideration, shown in Fig. 1, is a cantilevered microbeam with a wire loop deposited on its top surface. It will be assumed in the modeling of these devices that the mechanical effects of the wire loop are negligible because of the wire's small mass relative to the microbeam, and that the residual stress in the wire is minimal. In order to actuate the microbeam, the device is placed in a uniform magnetic field $\vec{B}$, which is at an angle α with respect to the vertical reference. When a current is supplied through the wire loop, the Lorentz force induces mechanical motion.

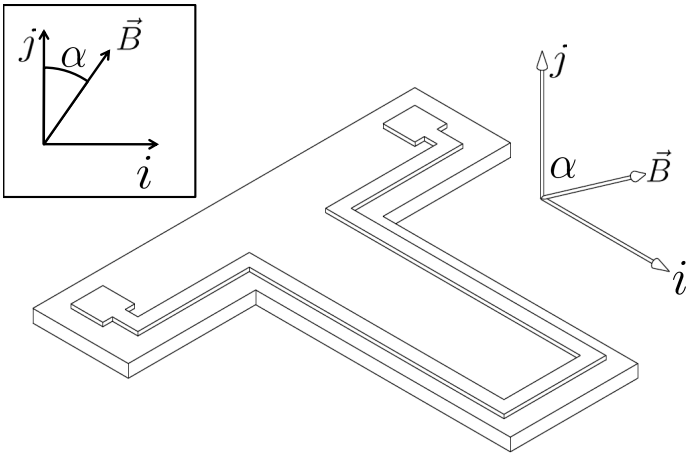

FIGURE 1. MODEL OF THE BEAM IN THREE DIMENSIONS. AS SHOWN IN THE INSET FIGURE, THE MAGNETIC FIELD $\vec{B}$ IS ORIENTED AT AN ANGLE α WITH RESPECT TO THE VERTICAL REFERENCE.

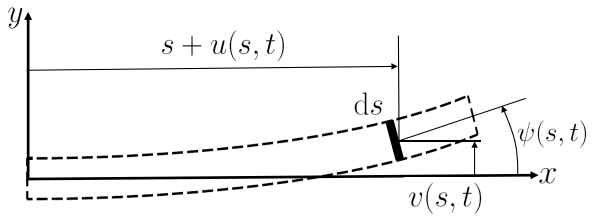

FIGURE 2. SCHEMATIC DIAGRAM OF THE BEAM ELEMENT WITH A DESCRIPTION OF THE VARIABLES USED FOR MODELING.

The variables used for the modeling of the microbeam are defined in Fig. 2. Using the Extended Hamilton's principle [19], a single degree of freedom governing equation for the microbeam can be developed. The specific Lagrangian of the microbeam is defined as

$$\bar{L} = \frac{1}{2}\int_0^l \rho A\left[\dot{u}^2+\dot{v}^2\right]\mathrm{d}s - \frac{1}{2}EI\psi'^2, \tag{1}$$

where u, v, and ψ are defined as in Fig. 2 and $(\dot{\bullet})$ and $(\bullet)'$ denote the derivatives with respect to the time and the arc length variable s respectively. The parameters of the microbeam are ρ, the beam density, A, the cross-sectional area, l, the undeformed length, E, the modulus of elasticity and I, the cross-sectional moment of inertia. Note that the rotational inertia of the microbeam is considered to be negligible because the thickness of the beam is much smaller than length of the beam. Assuming that shear deformations can be neglected and that deformation is primarily due to bending [20, 21], an inextensibility constraint and a kinematic constraint on the angle ψ can be developed

$$\begin{aligned}(1+u')^2+(v')^2 &= 1,\\ \tan\psi &= \frac{v'}{1+u'}.\end{aligned} \tag{2}$$

The variation of the Hamiltonian is given by

$$\begin{aligned}\delta H =& 0\\ =&\delta\int_{t_1}^{t_2}\int_0^l\left\{\bar{L}+\frac{1}{2}\lambda\left[1-(1+u')^2-(v')^2\right]\right\}\mathrm{d}s\mathrm{d}t\\ &+\int_{t_1}^{t_2}\int_0^l(Q_u\delta u+Q_v\delta v)\mathrm{d}s\mathrm{d}t,\end{aligned} \tag{3}$$

where λ is the Lagrange multiplier introduced to enforce the inextensibility constraint and Q_u and Q_v are planar, non-conservative forces in the u and v directions, respectively. Assuming that the microbeam is viscously damped and that the Lorentz force is a point load acting at the beam's free end, the non-conservative forces are given by

$$\begin{aligned}Q_u &= F_1\delta(s-l),\\ Q_v &= -c\dot{v}+F_2\delta(s-l),\end{aligned} \tag{4}$$

where c is the specific viscous damping coefficient and F_1 and F_2 are the resulting Lorentz forces in the longitudinal and transverse directions respectively. The equations governing the longitudinal and transverse displacement can be derived by first approximating u and ψ with a third-order Taylor series approximation by using the inextensibility constraint and the kinematic constraint on ψ, integrating Eqn. (3) successively by parts and finally applying the ideal cantilever boundary conditions. By solving for

the Lagrange multiplier in the equation governing the longitudinal displacement, and making the proper substitutions in the equation governing the transverse displacement, a single equation governing the transverse vibration can be recovered. This equation is nondimensionalized such that

$$\hat{v} = \frac{v}{v_0}, \quad \hat{s} = \frac{s}{l}, \quad \hat{t} = \frac{t}{T}, \tag{5}$$

where v_0 is the beam's thickness, and

$$T = \sqrt{\frac{\rho A l^4}{EI}}, \quad \hat{c} = \frac{cT}{\rho A}. \tag{6}$$

This yields a nondimensionalized, third-order, distributed-parameter model of the device given by

$$\begin{aligned}
&\frac{\partial^2 \hat{v}}{\partial \hat{t}^2} + \hat{c}\frac{\partial \hat{v}}{\partial \hat{t}} + \frac{\partial^4 \hat{v}}{\partial \hat{s}^4} + \frac{v_0^2}{l^2}\left(\frac{\partial^2 \hat{v}}{\partial \hat{s}^2}\right)^3 + 4\frac{v_0^2}{l^2}\frac{\partial \hat{v}}{\partial \hat{s}}\frac{\partial^2 \hat{v}}{\partial \hat{s}^2}\frac{\partial^3 \hat{v}}{\partial \hat{s}^3} \\
&+ \frac{v_0^2}{l^2}\left(\frac{\partial \hat{v}}{\partial \hat{s}}\right)^2 \frac{\partial^4 \hat{v}}{\partial \hat{s}^4} + \frac{1}{2}\frac{v_0^2}{l^2}\frac{\partial \hat{v}}{\partial \hat{s}}\frac{\partial^2}{\partial \hat{t}^2}\int_0^{\hat{s}}\left(\frac{\partial \hat{v}}{\partial \hat{s}_1}\right)^2 \mathrm{d}\hat{s}_1 \\
&+ \frac{1}{2}\frac{v_0^2}{l^2}\frac{\partial^2 \hat{v}}{\partial \hat{s}^2}\int_1^{\hat{s}}\frac{\partial^2}{\partial \hat{t}^2}\int_0^{\hat{s}_2}\left(\frac{\partial \hat{v}}{\partial \hat{s}_1}\right)^2 \mathrm{d}\hat{s}_1\mathrm{d}\hat{s}_2 \\
&+ \frac{l^2}{EI}\frac{\partial^2 \hat{v}}{\partial \hat{s}^2}\int_1^{\hat{s}} F_1(\hat{t})\delta(\hat{s}_1 - 1)\mathrm{d}\hat{s}_1 \\
&+ \frac{3}{2}\frac{v_0^2}{EI}\left(\frac{\partial \hat{v}}{\partial \hat{s}}\right)^2 \frac{\partial^2 \hat{v}}{\partial \hat{s}^2}\int_1^{\hat{s}} F_1(\hat{t})\delta(\hat{s}_1 - 1)\mathrm{d}\hat{s}_1 \\
&= \frac{l^3}{v_0 EI}F_2(\hat{t})\delta(\hat{s} - 1).
\end{aligned} \tag{7}$$

Using a Lorentz force model, the applied current and the force applied to the end of the microbeam are related by the following equation,

$$\vec{F}(\hat{t}) = i(\hat{t})\int \mathrm{d}\vec{l}\ \mathrm{x}\ \vec{B}, \tag{8}$$

where $i(\hat{t})$ is the applied current, and $\mathrm{d}\vec{l}$ is the differential element of the wire loop.

Defining the width of the wire loop to be g, the Lorentz force can be approximated as

$$\begin{aligned}
\vec{F}(\hat{t}) &= F_1(\hat{t})\mathbf{i} + F_2(\hat{t})\mathbf{j} \\
&= i(\hat{t})gB(\cos\alpha\mathbf{i} + \sin\alpha\mathbf{j}).
\end{aligned} \tag{9}$$

Assuming that the dynamics of the microbeam can be approximated by the first mode shape of an ideal cantilever according to

$$\hat{v}(\hat{s},\hat{t}) = z(\hat{t})\Psi(\hat{s}), \tag{10}$$

and projecting the model onto the first mode shape and subsequently rescaling time results in a final lumped-parameter governing equation given by

$$\begin{aligned}
&z'' + \varepsilon\bar{c}z' + [1 + \varepsilon\lambda_1 i(\tau)]z + [\varepsilon k_3 + \varepsilon\lambda_3 i(\tau)]z^3 \\
&\quad + \varepsilon\beta(zz'^2 + z^2 z'') = \eta_1 i(\tau).
\end{aligned} \tag{11}$$

The parameters used in Eqn. (11) are given in Table 1. Note that all of the parameters in Eqn. (11), except for η_1, are scaled by ε. ε is a small positive number assumed to be much less than one, which is used to not only imply the magnitude of a given parameter but also facilitates the application of various perturbation methods [22]. The specific order of ε is based on the physical parameters of the system, which are introduced later.

TABLE 1. DEFINITIONS OF THE NONDIMENSIONAL PARAMETERS USED IN EQN. (11).

$$\omega_0^2 = \int_0^1 \Psi\Psi^{iv}\mathrm{d}\hat{s}$$

$$\varepsilon\bar{c} = \frac{\hat{c}}{\omega_0}$$

$$\tau = \omega_0\hat{t}$$

$$(\bullet)' = \frac{\partial(\bullet)}{\partial\tau}$$

$$\varepsilon k_3 = \frac{v_0^2}{l^2\omega_0^2}\left(4\int_0^1 \Psi\Psi'\Psi''\Psi'''\mathrm{d}\hat{s} + \int_0^1 \Psi\Psi''^3\mathrm{d}\hat{s} + \int_0^1 \Psi\Psi'^2\Psi^{iv}\mathrm{d}\hat{s}\right)$$

$$\varepsilon\lambda_1 = \frac{gBl^2\cos\alpha}{EI\omega_0^2}\left(\int_0^1 \Psi\Psi''\int_1^{\hat{s}}\delta(\hat{s}_1 - 1)\mathrm{d}\hat{s}_1\mathrm{d}\hat{s}\right)$$

$$\varepsilon\lambda_3 = \frac{3v_0^2 gB\cos\alpha}{2EI\omega_0^2}\int_0^1 \Psi\Psi'^2\Psi''\int_1^{\hat{s}}\delta(\hat{s}_1 - 1)\mathrm{d}\hat{s}_1\mathrm{d}\hat{s}$$

$$\varepsilon\beta = \frac{v_0^2}{l^2}\left(\int_0^1 \Psi\Psi''\int_1^{\hat{s}}\int_0^{\hat{s}_2}\Psi'^2\mathrm{d}\hat{s}_1\mathrm{d}\hat{s}_2\mathrm{d}\hat{s} + \int_0^1 \Psi\Psi'\int_0^{\hat{s}}\Psi'^2\mathrm{d}\hat{s}_1\mathrm{d}\hat{s}\right)$$

$$\eta_1 = \frac{gBl^3\sin\alpha}{EIv_0\omega_0^2}\int_0^1 \Psi\delta(\hat{s} - 1)\mathrm{d}\hat{s}$$

Since a changing magnetic flux induces an electromotive force (emf), the vibrations of electromagnetic devices are coupled to the voltage potential across the device. By incorporating a second wire loop, the component of the voltage potential that is only dependent on the vibrations of the device can be isolated, thus allowing for self-sensing. The relationship between the emf and the response of the system can be obtained through a direct application of Faraday's Law [23, 24]. The magnetic flux $\Phi(t)$ through an arbitrary surface S is defined as

$$\begin{aligned}\Phi(t) &= \iint_S (\vec{B}\cdot\hat{n})\mathrm{d}S \\ &= \iint_S B\sin\alpha\sin\psi\mathrm{d}S + \iint_S B\cos\alpha\cos\psi\mathrm{d}S,\end{aligned} \tag{12}$$

where $\hat{n}$ is the unit vector normal to the surface. Note that the magnetic field $\vec{B}$ is assumed to be constant. Using a third-order Taylor series expansion for the terms with the angle ψ, nondimensionalizing and projecting the result onto the first mode, the flux through the device is approximated as

$$\begin{aligned}\Phi(\hat{t}) = &\left[Bg\sin\alpha v_0\int_0^1\Psi\int_0^1\Psi'\mathrm{d}\hat{s}\mathrm{d}\hat{s}\right]z \\ &+ Bg\cos\alpha l\int_0^1\Psi\mathrm{d}\hat{s} \\ &+ \left[\frac{Bg\cos\alpha v_0^2}{2l}\int_0^1\Psi\int_0^1\Psi'^2\mathrm{d}\hat{s}\mathrm{d}\hat{s}\right]z^2.\end{aligned} \tag{13}$$

Using Faraday's Law and rescaling time, the induced emf is defined as

$$\begin{aligned}V_{emf} &= -\frac{\partial\Phi(t)}{\partial t} \\ &= -\frac{1}{T\omega_0}\frac{\partial\Phi(\tau)}{\partial\tau}.\end{aligned} \tag{14}$$

Thus the lumped-mass approximation for the induced emf is

$$V_{emf} = \varepsilon^3\kappa_1 z' + \varepsilon^4\kappa_2 z z', \tag{15}$$

where

$$\begin{aligned}\varepsilon^3\kappa_1 &= -\frac{Bg\sin\alpha v_0}{T\omega_0}\int_0^1\Psi\int_0^1\Psi'\mathrm{d}\hat{s}\mathrm{d}\hat{s}, \\ \varepsilon^4\kappa_2 &= -\frac{Bg\cos\alpha v_0^2}{lT\omega_0}\int_0^1\Psi\int_0^1\Psi'^2\mathrm{d}\hat{s}\mathrm{d}\hat{s}.\end{aligned} \tag{16}$$

Note that the angle of the magnetic field α controls the linearity of the governing equation [Eqn. (11)] and the induced emf [Eqn. (15)]. When the magnetic field is parallel to the vertical reference, or $\alpha = 0$, the device is parametrically excited and the induced emf has a nonlinear relationship with the system's state. When the magnetic field is perpendicular to the vertical reference, or $\alpha = \pi/2$, the device is directly excited and the induced emf has a linear relationship with the system's velocity.

3 ISOLATED ELECTROMAGNETICALLY-ACTUATED MICROBEAM OSCILLATORS

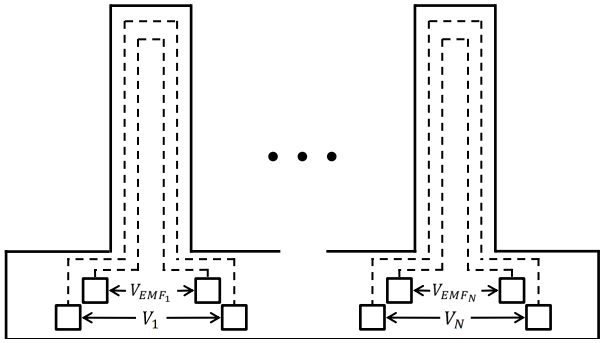

FIGURE 3. SCHEMATIC DIAGRAM OF AN ARRAY OF ELECTROMAGNETICALLY-ACTUATED MICROCANTILEVER OSCILLATORS. EACH MICROBEAM IS ASSUMED TO BE SPACED SUCH THAT THEY ARE MECHANICALLY ISOLATED. EACH MICROBEAM HAS TWO CURRENT LOOPS: ONE FOR ACTUATION AND ONE FOR SENSING.

A schematic diagram of the microbeam oscillators is shown in Fig. 3. The current design of the oscillators requires two wire loops per oscillator: the outer loop is for actuation and the inner loop is for sensing. Since this design requires at least four electrical contact pads per oscillator, methods to reduce the number of pads are currently being investigated. Note that it is assumed that all of the microbeams are spaced such that they are mechanically isolated.

As a preliminary step to understanding the dynamics of electromagnetically-actuated oscillator arrays, the dynamics of an isolated oscillator are considered. While the dynamics of oscillator arrays are more complicated than in the isolated case, many effects found in the isolated oscillators can still be found in the array. Through the use of feedback, the beam's actuation is dependent on the sensed emf, and therefore only the current state of the device. Thus under the conditions that will be detailed later in this section, the device can be made self-sustaining. For the isolated oscillator case, the following positive feedback control law is employed

$$V_c = \varepsilon^{-2}GV_{emf} - \varepsilon^{-2}K\left(\varepsilon^{-2}G\right)^3 V_{emf}^3, \tag{17}$$

where V_c is the controller voltage, $\varepsilon^{-2}G$ is the gain applied to the induced emf, and $\varepsilon^{-2}K$ is an additional gain used to adjust the oscillator amplitude. The controller voltage is related to the input current $i(\tau)$ by Ohm's Law

$$i(\tau) = \frac{V_c}{R}, \tag{18}$$

where R is the resistance of the actuation wire loop. This, in conjunction with a physically-consistent scaling results in a governing equation for the microbeam oscillator, truncated to third-order terms, given by

$$\begin{aligned} z'' + (\varepsilon\bar{c} - \varepsilon\gamma_1)z' + z + (\varepsilon^2\gamma_{21} - \varepsilon^2\gamma_{22})zz' + \varepsilon k_3 z^3 \\ + \varepsilon\beta(zz'^2 + z^2z'') + \varepsilon^3\gamma_3 z^2 z' + \varepsilon\gamma_4 z'^3 = 0, \end{aligned} \tag{19}$$

with parameters defined as in Table 2. Note that in these parameters, the εs are collected to reflect the relative magnitude of the parameters.

TABLE 2. DEFINITIONS OF THE PARAMETERS USED IN EQN. (19).

$$\begin{aligned} \varepsilon\gamma_1 &= \varepsilon\frac{G\kappa_1\eta_1}{R} \\ \varepsilon^2\gamma_{21} - \varepsilon^2\gamma_{22} &= \varepsilon^2\frac{G}{R}(\kappa_1\lambda_1 - \kappa_2\eta_1) \\ \varepsilon^3\gamma_3 &= \varepsilon^3\frac{G\kappa_2\lambda_1}{R} \\ \varepsilon\gamma_4 &= \varepsilon\frac{KG^3\kappa_1^3\eta_1}{R} \end{aligned}$$

In order to facilitate predictive design, the method of averaging can be used to calculate approximate solutions of Eqn. (19) [22, 25]. This equation is in the class of weakly-nonlinear oscillators, thus employing the following constrained coordinate transformation

$$\begin{aligned} z(\tau) &= a(\tau)\cos[\tau + \phi(\tau)], \\ z'(\tau) &= -a(\tau)\sin[\tau + \phi(\tau)], \end{aligned} \tag{20}$$

renders the slow flow equations given by

$$\begin{aligned} a'(\tau) &= \varepsilon\left[\frac{1}{2}(\gamma_1 - \bar{c})a - \frac{3}{8}\gamma_4 a^3\right] + O(\varepsilon^2) \\ \phi'(\tau) &= \varepsilon\left[\frac{1}{8}(3k_3 - 2\beta)a^2\right] + O(\varepsilon^2). \end{aligned} \tag{21}$$

Note that because of the scaling of the system, γ_{21}, γ_{22} and γ_3 do not appear in these equations. These terms are related to parametrically-excited feedback and the nonlinear effects in the emf respectively. The nonlinear differential equations presented in Eqn. (21) can be solved in closed form:

$$\begin{aligned} a &= \sqrt{\frac{a_0^2(\gamma_1 - \bar{c})}{\frac{3}{4}a_0^2\gamma_4 + [(\gamma_1 - \bar{c}) - \frac{3}{4}a_0^2\gamma_4]e^{-\varepsilon(\gamma_1 - \bar{c})\tau}}}, \\ \phi &= \phi_0 + \frac{3k_3 - 2\beta}{6\gamma_4}\ln\left[\frac{\frac{3}{4}a_0^2\gamma_4(e^{\varepsilon(\gamma_1 - \bar{c})\tau} - 1) + (\gamma_1 - \bar{c})}{\gamma_1 - \bar{c}}\right], \end{aligned} \tag{22}$$

where a_0 and ϕ_0 are the initial amplitude and phase. Note that these solutions evolve on a time scale slower than τ. Equation (22) shows that in order to have a stable limit cycle, $\gamma_1 > \bar{c}$ and $a_0 > 0$. Under these conditions, the steady-state solutions are given by

$$\begin{aligned} \hat{a} &= \lim_{\tau\to\infty} a(\tau) = \sqrt{\frac{4}{3}\frac{\gamma_1 - \bar{c}}{\gamma_4}}, \\ \hat{\phi} &= \lim_{\tau\to\infty} \phi(\tau) = \phi_0 + \frac{3k_3 - 2\beta}{3\gamma_4}\ln\left(\frac{a_0}{\hat{a}}\right) + \frac{3k_3 - 2\beta}{8}\hat{a}^2\tau. \end{aligned} \tag{23}$$

The steady-state amplitude $\hat{a}$ can be used to generate a bifurcation diagram of the system, which for the parameters in Table 3, $\alpha = \pi/4$ and $\varepsilon^{-2}K = 100$ is shown in Fig. 4. Note that $\varepsilon^{-2}G$, the gain applied to the emf, is negative such that γ_1 is positive. For the case shown in Fig. 4, the rest state, or zero solution, always exists, but is only stable for $\varepsilon^{-2}G$ greater than -3.701×10^3. When the magnitude of $\varepsilon^{-2}G$ is increased past this value, the oscillator has a stable limit cycle with a nonzero amplitude, provided the system has nonzero initial conditions.

A bifurcation diagram for $\varepsilon^{-2}G = -2 \times 10^4$ and $\varepsilon^{-2}K = 100$ is shown in Fig. 5. Similar to the previous case, the rest state is stable, provided that the magnitude of the magnetic field orientation angle is less than 0.309 rad. When the magnitude of the magnetic field orientation angle exceeds this value, the oscillator has a stable limit cycle with a nonzero amplitude provided the system has nonzero initial conditions. Also worth noting is that due to nonlinearities in the system there is a perturbation in the oscillation frequency.

4 TWO NEARLY-IDENTICAL MUTUALLY-COUPLED OSCILLATORS

The model for multiple oscillators can be derived from a modification of the control law for the microbeams. In the case where two microbeams are nearly-identical, the following con-

TABLE 3. DIMENSIONS AND MATERIAL PROPERTIES USED TO STUDY THE DYNAMIC RESPONSE OF A REPRESENTATIVE ELECTROMAGNETICALLY-ACTUATED MICROCANTILEVER OSCILLATOR.

Physical Parameter	Value
Length of Beam	400 μm
Width	50 μm
Thickness	2 μm
Young's Modulus (E)	159 GPa
Mass Density (ρ)	2330 kg/m^3
Magnetic Field Strength (B)	1 T
Quality Factor (Q)	500
Resistance (R)	30 Ω

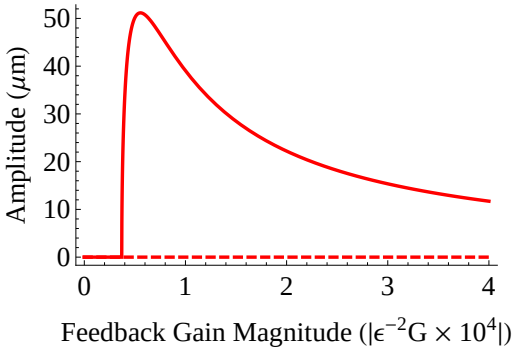

FIGURE 4. BIFURCATION DIAGRAM OF THE STEADY-STATE AMPLITUDE FOR THE PARAMETERS IN TABLE 3, $\alpha = \pi/4$ AND $\varepsilon^{-2}K = 100$. THE REST STATE ALWAYS EXISTS, HOWEVER IT IS ONLY STABLE FOR $\varepsilon^{-2}G$ GREATER THAN -3.701×10^3. FOR $\varepsilon^{-2}G$ LESS THAN THIS VALUE, THE SYSTEM HAS A STABLE LIMIT CYCLE.

trol laws are used:

$$
\begin{aligned}
i_1(\tau) &= \frac{V_{c1} + \varepsilon^{-2} G G_c V_{emf2}}{R}, \\
i_2(\tau) &= \frac{V_{c2} + \varepsilon^{-2} G G_c V_{emf1}}{R}.
\end{aligned}
\tag{24}
$$

Here, the subscript denotes the particular microbeam, G_c denotes a coupling gain, and all other quantities are defined as in the isolated scenario. The one addition to the model is that the microbeams have nearly-identical natural frequencies, where the square of the natural frequencies are $1 \pm 1/2\varepsilon\delta$ respectively. The governing equations used in the coupled case are therefore

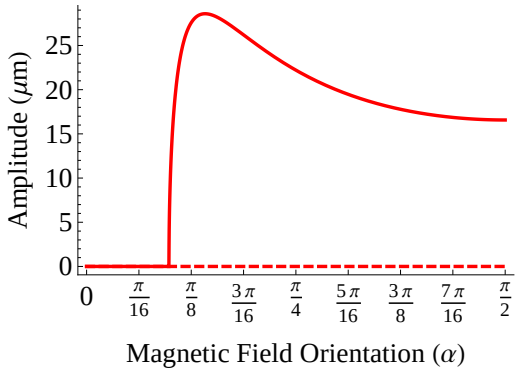

FIGURE 5. BIFURCATION DIAGRAM OF THE STEADY-STATE AMPLITUDE FOR THE PARAMETERS IN TABLE 3, $\varepsilon^{-2}G = -2 \times 10^4$ AND $\varepsilon^{-2}K = 100$. THE REST STATE ALWAYS EXISTS, HOWEVER IT IS ONLY STABLE FOR $|\alpha| < 0.309$. FOR α OUTSIDE THIS DOMAIN, THE SYSTEM HAS A STABLE LIMIT CYCLE.

$$
\begin{aligned}
&z_1'' + (\varepsilon\bar{c} - \varepsilon\gamma_1) z_1' - \varepsilon\gamma_1 G_c z_2' + (1 - \frac{\varepsilon\delta}{2}) z_1 \\
&\quad + (\varepsilon^2\gamma_{21} - \varepsilon^2\gamma_{22}) z_1 z_1' + \varepsilon^2\gamma_{21} G_c z_1 z_2' - \varepsilon^2\gamma_{22} G_c z_2 z_2' \\
&\quad + \varepsilon k_3 z_1^3 + \varepsilon\beta(z_1 z_1'^2 + z_1^2 z_1'') + \varepsilon^3\gamma_3 z_1^2 z_1' + \varepsilon\gamma_4 z_1'^3 \\
&\quad + \varepsilon^3\gamma_3 G_c z_1 z_2 z_2' = 0, \\
&z_2'' + (\varepsilon\bar{c} - \varepsilon\gamma_1) z_2' - \varepsilon\gamma_1 G_c z_1' + (1 + \frac{\varepsilon\delta}{2}) z_2 \\
&\quad + (\varepsilon^2\gamma_{21} - \varepsilon^2\gamma_{22}) z_2 z_2' + \varepsilon^2\gamma_{21} G_c z_2 z_1' - \varepsilon^2\gamma_{22} G_c z_1 z_1' \\
&\quad + \varepsilon k_3 z_2^3 + \varepsilon\beta(z_2 z_2'^2 + z_2^2 z_2'') + \varepsilon^3\gamma_3 z_2^2 z_2' + \varepsilon\gamma_4 z_2'^3 \\
&\quad + \varepsilon^3\gamma_3 G_c z_1 z_2 z_1' = 0.
\end{aligned}
\tag{25}
$$

Using first-order averaging and a slower time scale $\tau_1 = \varepsilon\tau$, solutions to the following slow flow equations provide solutions to Eqn. (25) to $O(\varepsilon)$

$$
\begin{aligned}
a_1'(\tau_1) &= \frac{1}{2}(\gamma_1 - \bar{c}) a_1 - \frac{3}{8}\gamma_4 a_1^3 + \gamma_1 \frac{G_c}{2} a_2 \cos(\phi_1 - \phi_2), \\
\phi_1'(\tau_1) &= -\frac{\delta}{4} + \frac{1}{8}(3k_3 - 2\beta) a_1^2 - \gamma_1 \frac{G_c}{2} \frac{a_2}{a_1} \sin(\phi_1 - \phi_2), \\
a_2'(\tau_1) &= \frac{1}{2}(\gamma_1 - \bar{c}) a_2 - \frac{3}{8}\gamma_4 a_2^3 + \gamma_1 \frac{G_c}{2} a_1 \cos(\phi_1 - \phi_2), \\
\phi_2'(\tau_1) &= \frac{\delta}{4} + \frac{1}{8}(3k_3 - 2\beta) a_2^2 + \gamma_1 \frac{G_c}{2} \frac{a_1}{a_2} \sin(\phi_1 - \phi_2).
\end{aligned}
\tag{26}
$$

Note that equations similar to the ones in Eqn. (26) have been extensively studied in prior literature, which can be utilized here [8]. As detailed in the following subsections, the solutions to Eqn. (26) can be classified as, stable rest state, symmetric phase locked, symmetric phase drift, and asymmetric phase locked. Since, in general, the conditions under which two oscillators are synchronized are of particular interest, a synchronized state is a phase locked state where $\psi' = \phi_1' - \phi_2' = 0$.

4.1 Stable Rest State Solutions

To solve for the conditions when the rest state, or state when oscillators have a zero amplitude, is stable, it is useful to transform the system in Eqn. (26) using the following coordinate transformation

$$u_1 + iv_1 = a_1 e^{i\phi_1}, \qquad u_2 + iv_2 = a_2 e^{i\phi_2}, \tag{27}$$

where the dynamic variables u_1, v_1, u_2 and v_2 are constrained to be real. Using these new coordinates, the slow-flow equations are given by

$$\begin{aligned}
u_1'(\tau_1) &= \frac{\delta}{4}v_1 + \frac{1}{2}(\gamma_1 - \bar{c})u_1 - \frac{3}{8}\gamma_4(u_1^3 + u_1 v_1^2) \\
&\quad - \frac{1}{8}(3k_3 - 2\beta)(u_1^2 v_1 + v_1^3) + \gamma_1 \frac{G_c}{2}u_2, \\
v_1'(\tau_1) &= -\frac{\delta}{4}u_1 + \frac{1}{2}(\gamma_1 - \bar{c})v_1 - \frac{3}{8}\gamma_4(u_1^2 v_1 + v_1^3) \\
&\quad + \frac{1}{8}(3k_3 - 2\beta)(u_1^3 + u_1 v_1^2) + \gamma_1 \frac{G_c}{2}v_2, \\
u_2'(\tau_1) &= -\frac{\delta}{4}v_2 + \frac{1}{2}(\gamma_1 - \bar{c})u_2 - \frac{3}{8}\gamma_4(u_2^3 + u_2 v_2^2) \\
&\quad - \frac{1}{8}(3k_3 - 2\beta)(u_2^2 v_2 + v_2^3) + \gamma_1 \frac{G_c}{2}u_1, \\
v_2'(\tau_1) &= \frac{\delta}{4}u_2 + \frac{1}{2}(\gamma_1 - \bar{c})v_2 - \frac{3}{8}\gamma_4(u_2^2 v_2 + v_2^3) \\
&\quad + \frac{1}{8}(3k_3 - 2\beta)(u_2^3 + u_2 v_2^2) + \gamma_1 \frac{G_c}{2}v_1.
\end{aligned} \tag{28}$$

The eigenvalues λ, of the Jacobian evaluated at the rest state, or $u_1 = v_1 = u_2 = v_2 = 0$, are

$$\lambda = \frac{1}{2}(\gamma_1 - \bar{c}) \pm \frac{1}{4}\sqrt{4\gamma_1^2 G_c^2 - \delta^2}. \tag{29}$$

The rest state is asymptotically stable when the real part of the eigenvalues are negative. Thus, the rest state is stable when $\bar{c} > \gamma_1$ and $|G_c| < \frac{1}{2}\sqrt{\frac{4(\bar{c}-\gamma_1)^2 + \delta^2}{\gamma_1^2}}$.

4.2 Symmetric Phase Locked Solutions

To determine the conditions when the oscillators are synchronized, the slow-flow equations in Eqn. (26) can be reduced from four equations to three by introducing a relative phase, $\psi = \phi_1 - \phi_2$.

$$\begin{aligned}
a_1'(\tau_1) &= \frac{1}{2}(\gamma_1 - \bar{c})a_1 - \frac{3}{8}\gamma_4 a_1^3 + \gamma_1 \frac{G_c}{2}a_2 \cos\psi, \\
a_2'(\tau_1) &= \frac{1}{2}(\gamma_1 - \bar{c})a_2 - \frac{3}{8}\gamma_4 a_2^3 + \gamma_1 \frac{G_c}{2}a_1 \cos\psi, \\
\psi'(\tau_1) &= -\frac{\delta}{2} + \frac{1}{8}(3k_3 - 2\beta)(a_1^2 - a_2^2) - \gamma_1 \frac{G_c}{2}\left(\frac{a_1}{a_2} + \frac{a_2}{a_1}\right)\sin\psi.
\end{aligned} \tag{30}$$

Since Eqn. (30) is symmetric with respect to the amplitude variables, assuming symmetric solutions of the form $a_1 = a_2 = a$ reduces Eqn. (30) to

$$\begin{aligned}
a'(\tau_1) &= \frac{1}{2}(\gamma_1 - \bar{c})a - \frac{3}{8}\gamma_4 a^3 + \gamma_1 \frac{G_c}{2}a\cos\psi, \\
\psi'(\tau_1) &= -\frac{\delta}{2} - \gamma_1 G_c \sin\psi.
\end{aligned} \tag{31}$$

Setting $a' = \psi' = 0$ reveals the solutions of interest. Note that the second equation of Eqn. (31) is independent of the amplitude and is a phase model for the synchronization of two oscillators. This equation has also been called Adler's equation [26] and is a form of the Kuramoto model for two oscillators. The phase equation only has constant solutions when

$$\left|\frac{\delta}{2\gamma_1 G_c}\right| \leq 1, \tag{32}$$

thus this condition must be met to have symmetric phase locked solutions. As such, in order to have synchronization, the beams must be nearly-identical or the coupling must be large enough to overcome the frequency mistuning.

Making the restriction that the only solutions of interest are $-\pi \leq \psi < \pi$, the steady-state solutions to Eqn. (31), given in (a, ψ) pairs with conditions on the damping and coupling, are

$$(\sqrt{\hat{a}^2 - a_c}, -\pi + \psi_c), \bar{c} < \gamma_1, G_{c1} < G_c < G_{c2} \tag{33}$$

$$(\sqrt{\hat{a}^2 - a_c}, -\psi_c), \bar{c} < \gamma_1, -G_{c2} < G_c < -G_{c1} \tag{34}$$

$$(\sqrt{\hat{a}^2 + a_c}, -\psi_c), \bar{c} < \gamma_1, G_{c1} < G_c \tag{35}$$

$$(\sqrt{\hat{a}^2 + a_c}, -\psi_c), \bar{c} > \gamma_1, G_{c2} < G_c \tag{36}$$

$$(\sqrt{\hat{a}^2 + a_c}, \pi + \psi_c), \bar{c} < \gamma_1, -G_{c1} > G_c \tag{37}$$

$$(\sqrt{\hat{a}^2 + a_c}, \pi + \psi_c), \bar{c} > \gamma_1, -G_{c2} > G_c \tag{38}$$

where

$$
\begin{aligned}
a_c &= \frac{2\sqrt{4\gamma_1^2 G_c^2 - \delta^2}}{3\gamma_4}, \\
\psi_c &= \arcsin\left(\frac{\delta}{2\gamma_1 G_c}\right), \\
G_{c1} &= \frac{\delta}{2\gamma_1}, \\
G_{c2} &= \frac{1}{2}\sqrt{\frac{4(\bar{c}-\gamma_1)^2+\delta^2}{\gamma_1^2}}.
\end{aligned}
\tag{39}
$$

In order to determine when these solutions are stable, the eigenvalues of the Jacobian of Eqn. (30), evaluated at the solutions given in Eqn. (33–38), are calculated. The eigenvalues, λ_i for i =1–3, in terms of a are

$$
\begin{aligned}
\lambda_1 &= -\frac{3\gamma_4 a^2}{4}, \\
\lambda_2 &= \gamma_1 - \bar{c} - \frac{3\gamma_4 a^2}{2}, \\
\lambda_3 &= \gamma_1 - \bar{c} - \frac{3\gamma_4 a^2}{4}.
\end{aligned}
\tag{40}
$$

Since a solution is stable if all of its eigenvalues have negative real parts, it can be shown that the solutions found in Eqn. (33) and Eqn. (34) are unstable and the solutions found in Eqn. (35–38) are stable.

4.3 Symmetric Phase Drift Solution

Since the phase equation in Eqn. (31) has no constant solutions when

$$
\left|\frac{\delta}{2\gamma_1 G_c}\right| > 1, \tag{41}
$$

there exists a symmetric phase drift solution only when this condition is satisfied. In order to facilitate a more direct analysis of this solution, the parameters used Eqn. (31) can be redefined so that they match a known problem [8]. Letting

$$
\begin{aligned}
\tau_2 &= \frac{3}{8}\gamma_4 \tau_1, \\
\Delta &= -\frac{4\delta}{3\gamma_4}, \\
\gamma &= \frac{4\gamma_1 G_c}{3\gamma_4}, \\
\kappa &= \frac{4(\bar{c}-\gamma_1)+3\gamma_4}{4\gamma_1 G_c},
\end{aligned}
\tag{42}
$$

Eqn. (31) can be written as

$$
\begin{aligned}
a'(\tau_2) &= a(1-\kappa\gamma-a^2)+\gamma a\cos\psi, \\
\psi'(\tau_2) &= \Delta - 2\gamma\sin\psi.
\end{aligned}
\tag{43}
$$

Equation (43) asymptotically approaches a limit cycle, which can be explicitly defined as

$$
\begin{aligned}
a(\tau_2) &= \sqrt{\frac{\hat{a}^2(1-d^2)}{1+d\sin(\psi+\theta+\pi)}}, \\
\psi(\tau_2) &= 2\arctan\left[\frac{\sqrt{\Delta^2-4\gamma^2}\tan\left(\frac{\tau_2\sqrt{\Delta^2-4\gamma^2}}{2}\right)+2\gamma}{\Delta}\right],
\end{aligned}
\tag{44}
$$

where

$$
\begin{aligned}
\hat{a}^2 &= 1-\kappa\gamma, \\
d &= \gamma/\sqrt{\hat{a}^4+\frac{1}{4}\Delta^2}, \\
\theta &= \arctan\left(\frac{2\hat{a}^2}{\Delta}\right).
\end{aligned}
\tag{45}
$$

The period of the limit cycle, T, can be explicitly defined

$$
T = \frac{2\pi}{\sqrt{\Delta^2-4\gamma^2}}, \tag{46}
$$

and the average value of the square of the amplitude over one period is the square of the uncoupled amplitude

$$
\frac{1}{T}\int_0^T a(\tau_2)^2 \mathrm{d}\tau_2 = \hat{a}^2. \tag{47}
$$

Since a periodic solution can be explicitly defined, the stability of the limit cycle can be determined from the Floquet multipliers of the first variation of the system evaluated on the limit cycle [27]. Specifically, if one of the Floquet multipliers is one and the others have a magnitude less than one, then the limit cycle is asymptotically stable. In order to more directly calculate the Floquet multipliers, another coordinate transformation and the parameters in Eqn. (43) can be used to manipulate Eqn. (30) such that

$$
\begin{aligned}
\sigma'(\tau_2) &= \sigma(\hat{a}^2-\gamma\cos\psi-3\zeta^2-\sigma^2), \\
\zeta'(\tau_2) &= \zeta(\hat{a}^2+\gamma\cos\psi-\zeta^2-3\sigma^2), \\
\psi'(\tau_2) &= \Delta+4q\sigma\zeta-2\gamma\frac{\zeta^2+\sigma^2}{\zeta^2-\sigma^2}\sin\psi,
\end{aligned}
\tag{48}
$$

where

$$\begin{aligned}\sigma &= \frac{1}{2}(a_1 - a_2),\\ \zeta &= \frac{1}{2}(a_1 + a_2),\\ q &= \frac{k_3 - \frac{2}{3}\beta}{\gamma_4}.\end{aligned} \tag{49}$$

The first variation of this system is given by

$$\begin{bmatrix}\sigma'\\ \zeta'\\ \psi'\end{bmatrix} = \begin{bmatrix}T_1 & 0 & 0\\ 0 & T_2 & -\gamma a \sin\psi\\ 0 & 0 & -2\gamma\cos\psi\end{bmatrix}\begin{bmatrix}\sigma\\ \zeta\\ \psi\end{bmatrix}, \tag{50}$$

where

$$\begin{aligned}T_1 &= \hat{a}^2 - \gamma\cos\psi - 3a^2,\\ T_2 &= \hat{a}^2 + \gamma\cos\psi - 3a^2,\end{aligned} \tag{51}$$

from which a fundamental solution matrix $\Phi(\tau_2)$ can be easily found, because the equations for σ and ψ are uncoupled. The Floquet multipliers, μ_i for $i = 1$–3, of Eqn. (50) can be found from the eigenvalues of $E = \Phi^{-1}(0)\Phi(T)$

$$\begin{aligned}\mu_1 &= \exp\left(-2\gamma\int_0^T \cos\psi\,\mathrm{d}\tau_2\right),\\ \mu_2 &= \exp\left(\int_0^T \hat{a}^2 - \gamma\cos\psi - 3a^2\,\mathrm{d}\tau_2\right),\\ \mu_3 &= \exp\left(\int_0^T \hat{a}^2 + \gamma\cos\psi - 3a^2\,\mathrm{d}\tau_2\right).\end{aligned} \tag{52}$$

Since the solution for ψ is periodic, the integral in μ_1 equals zero and $\mu_1 = 1$. Since a Floquet multiplier is equal to one, the limit cycle is stable if the following integral I is negative

$$I = \int_0^T \left(\hat{a}^2 - 3a^2\right)\mathrm{d}\tau_2. \tag{53}$$

The solution to this integral is given in [8] and $I = -4\pi\hat{a}^2/\sqrt{\Delta^2 - 4\gamma^2}$. For the limit cycle to exist, the radical term must be real and positive, thus the limit cycle is stable if $\hat{a} > 0$ or in terms of the parameters developed in the microbeam model, $\gamma_1 > \bar{c}$.

4.4 Asymmetric Phase Locked Solution

To determine the existence and stability of the asymmetric phase locked solution, consider the fixed points of the Eqn. (30) normalized by the parameters defined in the previous section

$$\begin{aligned}a_1'(\tau_2) &= a_1(\hat{a}^2 - a_1^2) + a_2\gamma\cos\psi,\\ a_2'(\tau_2) &= a_2(\hat{a}^2 - a_2^2) + a_1\gamma\cos\psi,\\ \psi'(\tau_2) &= \Delta + q(a_1^2 - a_2^2) - \gamma\left[\frac{a_1}{a_2} + \frac{a_2}{a_1}\right]\sin\psi.\end{aligned} \tag{54}$$

By equating the equations for $a_1'(\tau_2)$ and $a_2'(\tau_2)$ in Eqn. (54) to zero, solving for $\cos\psi$, then taking the ratio of the resulting equations, the asymmetric phase locked solution can be found to have the property that $\hat{a}^2 = a_1^2 + a_2^2$. Using this property of the asymmetric solution and all of the equations in Eqn. (54), the following relationships for the trigonometric functions can be developed

$$\begin{aligned}\cos\psi &= -\frac{a_1\sqrt{\hat{a}^2 - a_1^2}}{\gamma},\\ \tan\psi &= \frac{q(\hat{a}^2 - 2a_1^2) - \Delta}{\hat{a}^2}.\end{aligned} \tag{55}$$

Combining all of these results, the amplitude equation can be found

$$\gamma^2 = a_1^2\left(\hat{a}^2 - a_1^2\right)\left\{1 + \left[\frac{q(\hat{a}^2 - 2a_1^2) - \Delta}{\hat{a}^2}\right]^2\right\}. \tag{56}$$

The amplitude equation for the asymmetric solution only has solutions in the domain of $0 < a_1^2 < \hat{a}^2$. Solutions come in pairs such that if a solution is found, then $\hat{a}^2 = a_1^2 + a_2^2$ can be used to find the other solution. For small values of q only one pair of solutions exists, but for large values of q, two pairs of solutions can exist. To determine the stability of the asymmetric solution, consider the eigenvalues of the Jacobian evaluated at the asymmetric solution. Since the trace of the linearized system matrix is equal to zero, it is not possible for the system to be asymptotically stable. In addition, when $q = 0$, the determinant D of the linearized system matrix is

$$D = -2\hat{a}^2(\hat{a}^4 - 4\gamma^2 + \Delta^2). \tag{57}$$

Since this value is always negative when the solution exists, one eigenvalue has a negative real part and two have positive real parts. For the more general case when $q \neq 0$, the determinant of the linearized system matrix can be positive, negative and zero. In all of these cases however, it is not possible for all of the eigenvalues to have negative real parts. Thus, the asymmetric solution is not stable.

4.5 Bifurcation Diagrams

The following section details in a graphical fashion the different states the two oscillator system exhibits. For fixed values of $\varepsilon^{-2}G$, $\varepsilon^{-2}K$, α and δ, the amplitude of the oscillators are plotted against the coupling gain G_c in Fig. 6–7. The solutions are color coded: red identifies symmetric phase locked solutions, blue identifies symmetric phase drift solutions and black identifies asymmetric phase locked solutions. Note that the symmetric phase drift solutions are represented by the average value of the amplitude over one period. Stable solutions are solid lines and unstable solutions are dashed lines.

Figure 6 details the system's bifurcation structure when the frequency mistuning is $\delta = 0.05$ and the gain applied to the emf, $\varepsilon^{-2}G$, is below the threshold for an isolated oscillator to have a stable limit cycle. While the rest state solution always exists, it is only stable in the system highlighted in Fig. 6 when the magnitude of G_c is below a critical value of 15.422. When the magnitude of G_c exceeds this value, the symmetric phase locked solution is stabilized. Thus the coupling between the oscillators can be used to stabilize a synchronized solution, even when the isolated oscillators would have a stable rest state. Note that this behavior is the same in the case when there is no frequency mistuning, only in that scenario the coupling threshold is changed.

In the scenario shown in Fig. 7 there is no frequency mistuning, or $\delta = 0$, and the gain applied to the emf, $\varepsilon^{-2}G$, is above the threshold for an isolated oscillator to have a stable limit cycle, three types of solutions can exist. The rest state solution exists, but it is always unstable. Note that the stable rest state solution can only exist in systems where the isolated oscillators would not have a stable limit cycle. There are both stable and unstable symmetric phase locked solutions, but the stable solution always exists. Thus, unless the system has initial conditions that place the system on an unstable solution, this system will synchronize with the larger symmetric phase locked amplitude. Note that the asymmetric phase locked solution exists for values where the magnitude of the coupling gain is below a certain value, but this solution is never stable.

In the last case considered where G_c is varied, which is depicted in Fig. 8, the frequency mistuning has a nontrival value of $\delta = 0.05$ and the gain applied to the emf is above the threshold for an isolated oscillator to have a stable limit cycle. This case is similar to the previous one in that common solutions have qualitatively the same behavior, except an additional solution can exist, the symmetric phase drift solution. When the magnitude of the coupling gain G_c is below 0.771, the only stable solution is the symmetric phase drift solution. Depending on how close G_c is to this critical value controls how quickly the relative phase between the solutions drift. When the coupling is very weak, the behavior of the oscillators are very close to the scenario in which the oscillators are isolated. When the coupling is close to the critical coupling gain, the frequencies of the oscillators attempt to lock, but when the oscillators almost lock, one of the oscillators increases its frequency relative to the other. As the coupling gain increases beyond this critical value, a stable symmetric phase locked solutions always exists. For a smaller subset of values, two symmetric phase locked solutions can exist, however the smaller amplitude solution is never stable. The asymmetric phase locked solutions exists for values where the magnitude of the coupling gain is below a certain value, but these solutions are also never stable.

A potential application of nearly-identical, mutually-coupled oscillators is as a mass sensor. Assuming that only one of the microbeams is functionalized such that chemical agents are able to selectively bond to a microbeam, the addition of a small mass causes a shift in the natural frequency of the functionalized microbeam. Linear mass sensors require a system that is able to resolve these small changes in natural frequency, but frequency detuning between two mutually-coupled oscillators causes an amplitude and relative phase shift. Shown in Fig. 9 is the amplitude of the oscillators against δ when $\varepsilon^{-2}G$, $\varepsilon^{-2}K$, α and G_c are fixed. Note that same states are present as in Fig. 8. The symmetric phase locked solutions are stable when the magnitude of δ is less than 0.065, thus sensing amplitude shifts within this band of frequency detuning can be used to sense mass. A more direct way of sensing shifts in δ would be measuring the relative phase between the oscillators, which is nearly linear within this range of δ.

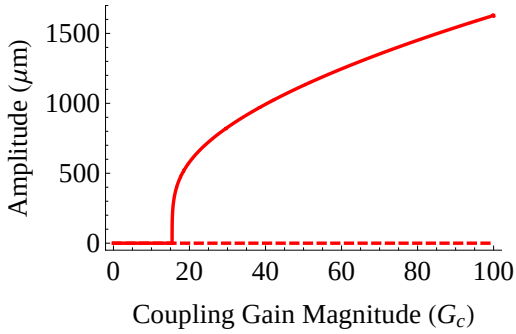

FIGURE 6. BIFURCATION DIAGRAM FOR THE TWO OSCILLATOR CASE WHEN $\bar{c} > \gamma_1$. THE PARAMETERS FOR THE SYSTEM ARE $\varepsilon^{-2}G = -3 \times 10^4$, $\varepsilon^{-2}K = 100$, $\alpha = \pi/4$ AND $\delta = 0.05$. THE REST STATE IS STABLE WHEN $|G_c| < 15.422$. WHEN G_c EXCEEDS THIS CRITICAL VALUE, THE SYMMETRIC PHASE LOCKED SOLUTION IS STABLE AND THE OSCILLATORS HAVE LIMIT CYCLES OF IDENTICAL FREQUENCY, WITH A PHASE DIFFERENCE RELATED TO THE FREQUENCY MISTUNING.

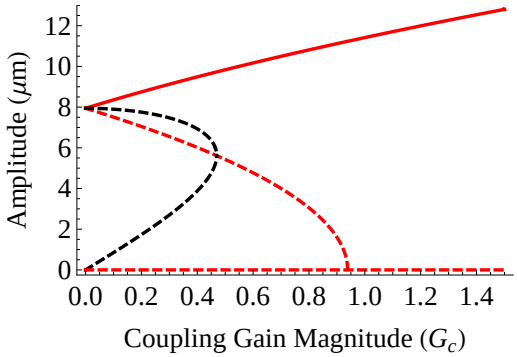

FIGURE 7. BIFURCATION DIAGRAM FOR THE TWO OSCILLATOR CASE, WITH $\varepsilon^{-2}G = -6\times10^5$, $\varepsilon^{-2}K = 100$, $\alpha = \pi/4$ AND $\delta = 0$. THE SOLUTIONS IN THIS CASE ARE QUALITATIVELY THE SAME AS IN THE CASE WHEN THERE IS A FREQUENCY MISTUNING, WITH TWO MAJOR DIFFERENCES: THE SYMMETRIC PHASE DRIFT SOLUTION DOES NOT EXISTS AND THE SYMMETRIC PHASE LOCKED SOLUTION IS ALWAYS STABLE FOR A NONZERO VALUE OF G_c.

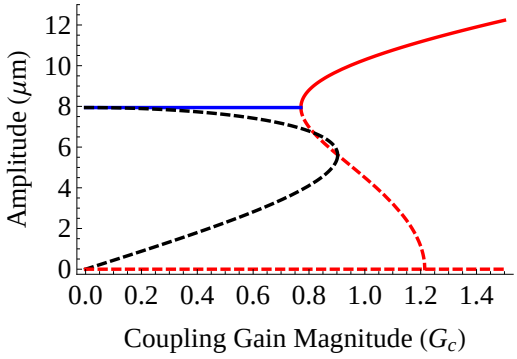

FIGURE 8. BIFURCATION DIAGRAM FOR THE TWO OSCILLATOR CASE, WITH $\varepsilon^{-2}G = -6\times10^5$, $\varepsilon^{-2}K = 100$, $\alpha = \pi/4$ AND $\delta = 0.05$. THE SYMMETRIC PHASE DRIFT SOLUTION (SOLID BLUE) IS THE ONLY STABLE SOLUTION WHEN $|G_c| < 0.771$. FOR LARGER G_c, THE ONLY STABLE SOLUTION IS THE LARGER SYMMETRIC PHASE LOCKED SOLUTION (SOLID RED). THE ASYMMETRIC (BLACK DASHED) AND SMALLER PHASE LOCKED SOLUTIONS (RED DASHED) EXIST FOR CERTAIN VALUES OF G_c, BUT THESE SOLUTIONS ARE NOT STABLE.

5 CONCLUSIONS AND FUTURE DIRECTIONS

In this work, the model of self-excited oscillators and associated arrays, composed of electromagnetically-actuated microbeam resonators with self-sensing capabilities, is developed. This model is analyzed, which produces predictive design methods based on the characterization of the nonlinear behaviors of the isolated and nearly-identical mutually-coupled oscillators.

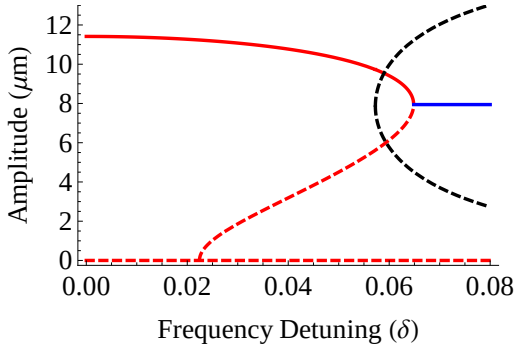

FIGURE 9. BIFURCATION DIAGRAM FOR THE TWO OSCILLATOR CASE, WITH $\varepsilon^{-2}G = -6\times10^5$, $\varepsilon^{-2}K = 100$, $\alpha = \pi/4$ AND $G_c = 1$. THE LARGER SYMMETRIC PHASE LOCKED SOLUTION IS THE ONLY STABLE SOLUTION FOR $|\delta| < 0.065$ AND OUTSIDE THIS RANGE THE SYMMETRIC PHASE DRIFT SOLUTION IS THE ONLY STABLE SOLUTION. SENSING THE AMPLITUDE OF THE PHASE LOCKED SOLUTION COULD BE EXPLOITED TO IMPLEMENT A MASS SENSOR.

Future work will not only consider the dynamics of larger oscillator arrays with different forms of coupling and feedback, but also experimental validation of the proposed model. Practical applications of these devices range from signal processing to micromechanical neurocomputing.

ACKNOWLEDGEMENTS

This material is based in part upon work supported by the National Science Foundation under Grant Number 0846385. Any opinions, findings, and conclusions or recommendations expressed in this material are those of the authors and do not necessarily reflect the views of the National Science Foundation.

REFERENCES

[1] Aubin, K., Zalalutdinov, M., Alan, T., Reichenbach, R., Rand, R., Zehnder, A., Parpia, J., and Craighead, H., 2004. Limit cycle oscillations in CW laser-driven NEMS. *Journal of Microelectromechanical Systems*, **13**(6), pp. 1018-1026.

[2] Zalalutdinov, M., Aubin, K. L., Pandey, M., Zehnder, A. T., Rand, R. H., Craighead, H. G., Parpia, J. M., and Houston, B. H., 2003. Frequency entrainment for micromechanical oscillator. *Applied Physics Letters*, **83**(16), pp. 3281-3283.

[3] Salvia, J. C., Melanud, R., Chandorkar, S. A., Lord, S. F. and Kenny, T. W., 2010. Real-Time Temperature Compensation of MEMS Oscillators Using an Integrated Micro-Oven and a Phase-Locked Loop. *Journal of Microelectromechanical Systems*, **19**(1), pp. 192–201.

[4] Nguyen, C. T.-C., 2007. MEMS technology for timing and

frequency control. *IEEE Transactions on Ultrasonics, Ferroelectrics, and Frequency Control*, **54**(2), pp. 251–270.

[5] Pikovsky, A., Rosenblum, M. and Kurths, J., 2001. *Synchronization: A Universal Concept in Nonlinear Sciences*. Cambridge University Press.

[6] Cross, M. C. , Rogers, J. L. , Lifshitz, R. and Zumdieck, A., 2006. Synchronization by reactive coupling and nonlinear frequency pulling. *Physical Review E*, **73**, 036205.

[7] Mendelowitz, L., Verdugo, A., and Rand, R., 2009. Dynamics of three coupled limit cycle oscillators with application to artificial intelligence. *Communications in Nonlinear Science and Numerical Simulation*, **14**(1), pp. 270–283.

[8] Aronson, D. G. , Ermentrout, G. B. and Kopell, N., 1990. Amplitude response of coupled oscillators. *Physica D*, **41**(3), pp. 403–449.

[9] Ivanchenko, M. V., Osipov, G. V., Shalfeev, V. D., and Kurths, J., 2004. Synchronization of two non-scalar-coupled limit-cycle oscillators. *Physica D*, **189**(1-2), pp. 8–30.

[10] Kuznetsov, A. P. and Roman, J. P., 2009. Properties of synchronization in the systems of non-identical coupled van der Pol and van der Pol-Duffing oscillators: broadband synchronization. *Physica D*, **238**(16), pp. 1499–1506.

[11] Ha, S. Y. , Ha, T. and Kim, J. H., 2010. On the complete synchronization of the Kuramoto phase model. *Physica D*, **239**(17), pp. 1692–1700.

[12] Acebron, J. A., Bonilla, L. L., Perez Vicente, C. J., Ritort, F. and Spigler, R., 2005. The Kuramoto model: A simple paradigm for synchronization phenomena. *Review of Modern Physics*, **77**(1), pp. 137–185.

[13] Pandey, M., Rand, R. and Zehnder, A., 2007. Perturbation analysis of entrainment in a micromechanical limit cycle oscillator. *Communications in Nonlinear Science and Numerical Simulation*, **12**(7), pp. 1291–1301.

[14] Strogatz, S. H., 2000. From Kuramoto to Crawford: Exploring the onset of synchronization in populations of coupled oscillators. *Physica D*, **143**(1-4), pp. 1–20.

[15] Liao, P. and York, R. A., 1993. A new phase-shifterless beam-scanning technique using arrays of coupled oscillators. *IEEE Transactions on Microwave Theory and Techniques*, **41**(10), pp. 1810–1815.

[16] August, E. and Barahona, M., 2011. "Obtaining Certificates for Complete Synchronisation of Coupled Oscillators". *Physica D*, **240**(8), pp. 795–803.

[17] Hoppensteadt, F. C. and Izhikevich, E. M., 2001. Synchronization of MEMS resonators and mechanical neurocomputing. *IEEE Transactions on Circuits and Systems I: Fundamental Theory and Applications*, **48**(2), pp. 133–138.

[18] Chang, H.–C., Cao, X., Mishra, U. K. and York, R. A., 1997. Phase Noise in Coupled Oscillators: Theory and Experiment. *IEEE Transactions on Microwave Theory and Techniques*, **45**(5), pp. 604–615.

[19] Meirovitch, L., 1970. *Methods of Analytical Dynamics*. McGraw-Hill Book Company.

[20] Baillieul, J. and Levi M., 1991. "Constrained Relative Motions in Rotational Mechanics". *Archive for Rational Mechanics and Analysis*, **115**(2), pp. 101–135.

[21] Crespo Da Silva, M. R. M., 1978. "Flexural-Flexural Oscillations of Becks's Column Subjected to a Planar Harmonic Excitation". *Journal of Sound and Vibration*, **60**(1), pp. 133-144.

[22] Nayfeh, A. H. and Mook, D. T., 1995. *Nonlinear Oscillations*. Wiley-Interscience.

[23] Jackson, J. D., 1962. *Classical Electrodynamics*. John Wiley & Sons.

[24] Matveyey, A., 1966. *Principles of Electrodynamics*. Reinhold Publishing Company.

[25] Sanders, J. A., Verhulst, F. and Murdock, J., 2007. *Averaging Methods in Nonlinear Dynamical Systems*. Springer.

[26] Adler, R., 1973. "A Study of Locking Phenomena in Oscillators". *Proceedings of IEEE*, **61**(10), pp. 1380-1385.

[27] Coddington, E. A. and Levison, N., 1955 *Theory of Ordinary Differential Equations*. McGraw-Hill.